



Catalytic wet air oxidation of high BPA concentration over iron-based catalyst supported on orthophosphate

Fatiha Kaissouni, Rachid Brahmi, Mohamed Zbair, Gwendoline Lafaye, Zouhair El Assal, Laurence Pirault-Roy, Jacques Barbier Jr, Abdelkrim Elaissi, Mohammed Bensitel, Mohammed Baalala

► To cite this version:

Fatiha Kaissouni, Rachid Brahmi, Mohamed Zbair, Gwendoline Lafaye, Zouhair El Assal, et al.. Catalytic wet air oxidation of high BPA concentration over iron-based catalyst supported on orthophosphate. *Environmental Science and Pollution Research*, 2020, 27 (26), pp.32533-32543. <10.1007/s11356-020-09176-3>. <hal-03533602>

HAL Id: hal-03533602

<https://hal.science/hal-03533602v1>

Submitted on 22 Mar 2023

HAL is a multi-disciplinary open access archive for the deposit and dissemination of scientific research documents, whether they are published or not. The documents may come from teaching and research institutions in France or abroad, or from public or private research centers.

L'archive ouverte pluridisciplinaire **HAL**, est destinée au dépôt et à la diffusion de documents scientifiques de niveau recherche, publiés ou non, émanant des établissements d'enseignement et de recherche français ou étrangers, des laboratoires publics ou privés.



HAL Authorization

Catalytic Wet Air Oxidation of High BPA Concentration Over Iron based Catalyst Supported on Orthophosphate

Fatiha Kaissouni¹, Rachid Brahmi^{2*}, Mohamed Zbair¹, Gwendoline Lafaye⁴, Zouhair El Assal³, Laurence Pirault-Roy⁴, Jacques Barbier Junior⁴, Abdelkrim Elaissi¹, Mohammed Bensitel¹, Mohammed Baalala¹

¹Laboratory of Catalysis and Corrosion of Materials, Department of Chemistry, University Chouaïb Doukkali, Avenue des Facultés, 24000 El Jadida -Morocco.

²Laboratory of Coordination and Analytical Chemistry (LCCA), University Chouaïb Doukkali, Avenue des Facultés, 24000 El Jadida -Morocco.

³Faculty of Technology, Environmental and Chemical Engineering, University of Oulu, P. O. Box 4300, FI-90014 Oulu, Finland.

⁴IC2MP UMR 7285 CNRS, University of Poitiers, 4 rue Michel Brunet, 86022 Poitiers Cedex, France.

* Corresponding author: rachid.brahmi@univ-poitiers.fr

Acknowledgments

We gratefully acknowledge the financial support provided by the European communities (FEDER), the “Région Nouvelle Aquitaine”, and the Project Partenariats Hubert Curien (PHC) Maghreb program (16MAG11) for funding Miss Kaissouni's internships at IC2MP, Poitiers-France.

Abstract

The catalytic performance of Fe supported on nickel phosphate (NiP) was evaluated for the removal of Bisphenol A (BPA) by catalytic wet air oxidation (CWAO) at 140°C and 25 bar of pure oxygen pressure. The prepared NiP and Fe/NiP materials were fully characterized by XRD, N₂-physisorption, H₂-TPR, TEM, and ICP analysis. Iron (Fe/NiP) impregnation of NiP support enhanced the BPA removal efficiency from 37.0 % to 99.6 % when CWAO was performed. This catalyst was highly stable given the operating conditions of acidic medium, high temperature and high pressure. The Fe/NiP catalyst showed an outstanding catalytic activity for oxidation of BPA, achieving almost complete removal of BPA in 180 min at a concentration of 300 mg/L, using 4 g/L of Fe/NiP. No iron leaching was detected after the CWAO of BPA. The stability of Fe/NiP was performed over three consecutive cycles, noting that BPA conversion was not affected and iron leaching was negligible. Therefore, this catalyst (Fe/NiP) could be considered as an innocuous and effective long-lasting catalyst for the oxidation of harmful organic molecules.

Keywords: Bisphenol A; CWAO; Oxidation; Catalyst; iron-Nickel Phosphate; Environment.

Abbreviations:

WAO	: Wet Air Oxidation
CWAO	: Catalytic Wet Air Oxidation,
BPA	: Bisphenol A,
EDC	: Endocrine Disrupting Chemical
AOPs	: Advanced Oxidation Processes,
XRD	: X-Ray Diffraction,
H₂-TPR	: Temperature-Programmed Reduction,
ICP-OES	: Inductively Coupled Plasma Optical Emission Spectroscopy,
TEM	: Transmission Electron Microscopy,
TOC	: Total Organic Carbon,
COD	: Chemical Oxygen Demand,
HPLC	: High Performance Liquid Chromatography,
PFO	: Pseudo-First-Order.

1. Introduction

Bisphenol A (BPA) is a synthetic organic compound with two unsaturated phenolic rings attached by a bridging carbon. BPA is classified as an endocrine-disrupting chemical (EDC) with estrogenic properties, but it is still widely used as a plasticizer in the synthesis of polycarbonate plastics and epoxy resins (Ben-Jonathan and Steinmetz, 1998) because it is very durable; heat and shatter resistant, and can also improve the clarity of plastics. It is widely used in the manufacture of some food and beverage packaging, e.g., water and baby bottles, compact discs, dental sealants, medical devices and lacquers for coating metal products such as plastic cans, bottle caps and water pipes (Chapin et al., 2008; Chouhan et al., 2014). Thus, humans ingest BPA on an almost daily basis. It is known that babies and children are more affected by BPA than adults. BPA has been detected in urine and serum of pregnant women and in placental tissue, amniotic fluid and urine of babies (Vandenberg et al., 2007). In addition, BPA has also been detected in wastewater, groundwater, surface water and even drinking water (Lane et al., 2015; Lee et al., 2015; Zbair et al., 2018). Recent studies have indicated that the estrogenic activity of BPA at levels as low as 0.2 pg/mL causes endocrine disruption leading in infertility, breast cancer and thyroid cancer (Gültekin and Ince, 2007). There is therefore an urgent need to develop effective technology to remove BPA from wastewater and drinking water.

Up to date, a number of methods such as adsorption, biological treatment and advanced oxidation have been investigated to remove BPA from water (Anastopoulos et al., 2017; Mohapatra et al., 2010; Zbair et al., 2018). Biological treatment would be the least expensive, but it takes longer to remove BPA (Lobos et al., 1992; Omoike et al., 2013). Moreover, conventional biological management appears to have a low and unstable BPA removal capacity due to its very low concentration in water and high biorefractory properties (Cleveland et al., 2014; Staples et al., 1998). The adsorption process is simple and efficient, but it requires high operating costs related to the regeneration of spent adsorbents from contaminants (Cleveland et al., 2014). On the other hand, advanced oxidation processes (AOPs) have demonstrated a great capacity to degrade persistent organic matter through the formation of highly active oxidizing free radicals (HO and SO_4^-) (Athalthil et al., 2015; Reddy and Kim, 2015). Among the processes of AOPs tested for the elimination of BPA, it can be mentioned: UV/ H_2O_2 process (Moussavi et al., 2018), electro-generated ferrous ion activated ozone, H_2O_2 and persulfate system (Akbari et al., 2016), Fenton like process (Ahmadi et al., 2016; Arampatzidou et al., 2018) and catalytic wet air oxidation (CWAO) method (Erjavec et al., 2013). CWAO is a particularly effective and promising process for removing organic compounds, such as phenolic compounds, from wastewater (Keav et al., 2014;

Nousir et al., 2008). Moreover, CWA0 is an industrially feasible and environmentally-friendly system that destroys organic contaminants as biodegradable intermediates or mineralizes them into CO₂, H₂O and harmless end-products at high temperature (125–320 °C) and under oxygen or air pressure (0.5–20 MPa). Noble metals supported on oxides or carbon materials are widely studied in CWA0 because of their high catalytic performance and resistance to metal leaching (Kim and Ihm, 2011; Levec and Pintar, 2007). However, the high cost and scarcity of these precious metals make it necessary to explore new routes to either minimize their use or replace them with non-noble catalysts with similar catalytic properties. Phosphate-based materials have been of great interest in recent years as they can be used as fertilizers, catalysts, ion conductors, piezoelectric materials, biotechnological materials and sorbents. Currently, there is more interest in the use of these materials as catalysts for various chemical transformations.

The titanate nanotube-based catalyst proved to be very efficient for the destruction of BPA by CWA0 exhibiting a high activity around 91 %, and 69 % of TOC removal (Kaplan et al., 2014a). The resulted end-product solution contained small amounts of biodegradable compounds.

Moreover the CeO₂ and Ce_{0.85} Zr_{0.15}O₂ CWA0 based catalysts reaches 76 % of BPA removal and respectively 75 % and 73% of TOC abatement (Heponiemi et al., 2015).

The novelty of this research is the investigation of inexpensive Iron-Nickel-Phosphate oxide based catalysts in the catalytic wet air oxidation of an aqueous solution of Bisphenol A. The activity of the catalyst (Fe/NiP) and its stability were studied for the removal of Bisphenol A (BPA) by catalytic wet air oxidation (CWA0). The objective is to identify the features of the catalyst that will influence the activity and selectivity of the reaction.

2. Materials and methods

2.1. Preparation of nickel phosphate support (NiP)

The support was prepared by co-precipitation method using the required stoichiometric amount of aqueous solutions of the precursor salts Ni(NO₃)₂·6 H₂O (Sigma-Aldrich Chemical company, 99% purity) and (NH₄)₂HPO₄ (Sigma-Aldrich chemical Company, 99% purity).. The salt solution of Ni(NO₃)₂·6 H₂O is added drop by drop on the ammonium hydrogenophosphate solution under continuous stirring. The pH was then adjusted to 9 with ammonia solution (25%, Sigma-Aldrich chemical Company) and the mixture was left under constant stirring for 3 hours. The obtained co-precipitate solid was dried overnight at 120°C and calcined under air flow at 450°C for 8 hours with a temperature rise of 5 ° C min⁻¹. The resulting support was labeled NiP.

2.2. Deposition of the iron active phase

The wet-impregnation method was used to deposit 20 wt-% of iron from an aqueous solution of $\text{FeSO}_4 \cdot 7 \text{H}_2\text{O}$ (Sigma-Aldrich, 99%). The support is brought into contact with the necessary volume of iron solution. The mixture of Fe precursor solution and the support was stirred overnight and dried at 60°C until the excess water evaporated completely. Finally, the dried sample was calcined in an air atmosphere for 3 hours at 450°C with a ramp of 5°C min^{-1} .

2.3. Characterization methods

The X-ray diffraction (XRD) analysis of NiP and Fe/NiP was performed using a Bruker-BINARY, model D8 Diffractometer, equipped with a $\text{Cu K}\alpha$ radiation ($\lambda_{\text{K}\alpha} = 1.5418 \text{ \AA}$). Both samples were scanned in the range 2θ from 15° to 70° with a 0.02° step in 30 s.

The specific surface areas, pore volume and pore size distribution of NiP and Fe/NiP were measured by nitrogen physisorption at -196°C using a Micrometrics TRISTAR 3000 device applying successively the BET and the BJH models. Prior to these measurements, the samples were degassed under vacuum at 250°C overnight to clean the surface of the materials.

H_2 -TPR (temperature-programmed reduction) measurements were performed on an Autochem II 2920 with a 10% H_2/Ar gas mixture and a flow rate set at 50 mL/min. Prior to the measurements, the samples were pretreated under Ar at 450°C for 1h, with a temperature ramp of 10°C/min , and then cooled down to room temperature. H_2 -TPR analysis was performed from room temperature to 850°C with a ramp of 10°C/min .

The Fe content of the prepared catalyst (Fe/NiP) was determined by inductively coupled plasma optical emission spectroscopy (ICP-OES). The analysis was performed using a Perkin-Elmer Optima 2000DV. Prior to analysis, a known mass of sample powder was dissolved in acid under microwave heating. The ICP analysis was also used to analyze the leaching of iron in aqueous solution after CWAO reaction.

The surface morphology of NiP and Fe/NiP were observed by transmission electron microscopy using a "TEM / STEM JEOL 2100 UHR", with a resolution of 0.19 nm, equipped with an EDAX energy dispersive spectrometer, a HAADF wide angle annular dark field detector and Gatan CCD camera.

2.4. Catalytic experiments

CWAO experiments were investigated in a 0.44 L batch reactor made of Hastelloy C22 alloy loaded with 160 mL of BPA solution (0.3 g/L) and NiP or Fe/NiP catalyst (4 g/L). After a purge with helium, the reactor was heated up to the reaction temperature. The stirring speed was set at 1000 rpm. At the initial time of the reaction, 25 bars of pure O_2 were introduced into the reactor. The

pressure was kept constant during the experiment by regular refilling with O₂. Samples of the liquid phase were periodically collected and filtered through a Durapore membrane (0.45 µm; Ø = 13 mm) to remove all catalyst residues for analysis. The liquid samples were analyzed by HPLC using a 250 × 4.6 mm C18 reversed-phase column (Shimadzu Prominence UFLC_{XR}). The mobile phase was a mix of 60 vol. % methanol and 40 vol. % water (flow rate: 0.8 mL/min). The HPLC system was equipped with a UV-visible detector fixed at 276 nm. Total Organic Carbon (TOC) values were determined using a total organic analyzer Shimadzu LCPH/CPN. The HPLC and TOC devices are calibrated using standard solutions of Bisphenol A in ultra-pure water. At the end of the CWAO reaction (180 min), the reactor was cooled down to room temperature. ICP analysis of the remaining solutions was performed to ensure that iron did not leach from the Fe/NiP catalyst. It is worth noted that the reproducibility of the experimental protocol was proved for several reference catalysts and that the experimental error was found to be less than 5%.

3. Results and Discussion

3.1.Characterization of samples

X-ray diffraction was used to identify crystalline phases formed in NiP support and Fe/NiP catalyst. **Fig. 1a** shows the XRD patterns of NiP and Fe/NiP samples which display amorphous phases and semi-crystalline peaks. By comparison with ICDD database (International Centre for Diffraction Data), it appears that the main crystalline phase on the NiP support is a monoclinic structure of Ni₃(PO₄)₂ (ICDD: 00-038-1473). As expected, the XRD pattern of Fe/NiP catalyst reveals the presence of Ni₃(PO₄)₂ phase. It presents also a hydrated phase of iron sulfate hydroxide ((Fe_{1.33}²⁺Fe_{0.67}³⁺(SO₄)₂(OH)_{0.67}·xH₂O) (ICDD: 00-053-1056), as well as unidentified phases. The amount of iron impregnated on NiP support, determined by ICP analysis, is 18.5 wt-% (**Table 1**), which is close to the target value (20 wt-%).

According to IUPAC Classification (Sing, 1985) , the N₂-physorptions on NiP and Fe/NiP evidence type IV isotherms indicating the presence of mesopores (**Fig. 1b**). Both isotherms exhibit type H3 hysteresis loop, indicating the presence of non-rigid aggregates of plate-like particles or assemblages of slit-like pores.

For comparison purposes, the specific surface area, the total pore volume, and the average pore diameter obtained from nitrogen physisorption isotherms of NiP and Fe/NiP are summarized in **Table 1**. All the textural parameters decrease after the impregnation of iron, suggesting that iron particles partially block NiP support pores.

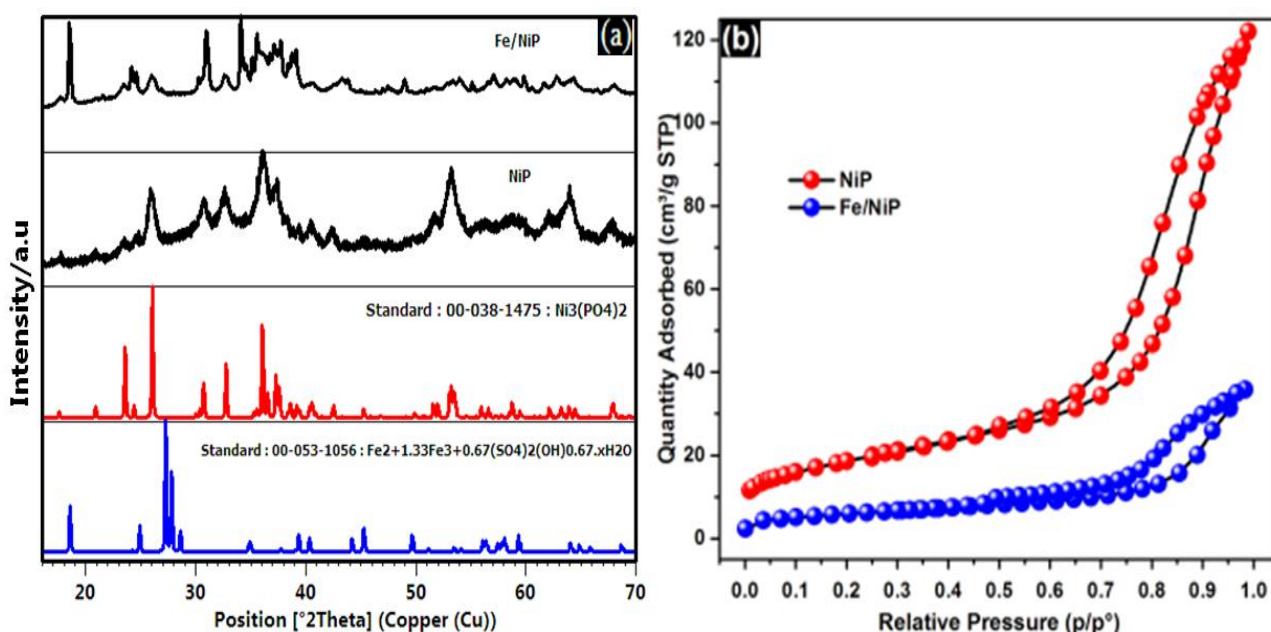


Fig. 1: XRD patterns (a) and Nitrogen adsorption-desorption isotherms (b) of NiP and Fe/NiP.

Table 1. Textural parameters and ICP analysis of NiP and Fe/NiP.

Sample	S _{BET} (m ² /g)	Total pore volume (cm ³ /g)	Average pore diameter (nm)	Fe Content (wt-%)
NiP	66	0.18	10.8	-
Fe/NiP	21	0.05	9.2	18.5

H₂-Temperature Programmed Reduction (H₂-TPR) was performed on the samples. **Fig. 2** shows the hydrogen uptakes as a function of temperature, obtained for NiP (**Fig. 2a**) and Fe/NiP (**Fig. 2b**). The decomposition of the TPR profile of NiP reveals several peaks located around 407, 444, 543, 645, 725, 781, and 820 °C (**Fig. 2a**). According to the literature, the peaks at 407 °C and 444 °C can be attributed to the reduction of small and large crystallites of NiO to Ni metallic, respectively (Bui et al., 2012; Chen et al., 2014; Pan et al., 2016; Zou et al., 2018). The peak at 543 °C is related to the phosphidation of nickel (Bui et al., 2012). Furthermore, the peak at 645 °C can be assigned to the reduction of nickel oxy-phosphate (Chen et al. 2014). In addition, the peaks at 725, 781, and 820 °C could be due to the reduction of nickel oxy-phosphate, nickel phosphate and P-O bond (Bui et al., 2012; Chen et al., 2014; Pan et al., 2016).

Fig. 2b shows that the addition of iron to NiP strongly modifies the shape of the TPR profile of NiP (**Fig. 2a**). Decomposed TPR curve of Fe/NiP displays four peaks at 460, 482, 524 and 770 °C. The reduction temperature of NiO to metallic Ni shifts slightly to a higher temperature in the presence of Fe. This slight increase from 444 °C to 460 °C is consistent with the literature (Zou et al., 2018) and

is explained by an interaction between Ni and Fe. The peak at 482 °C can be assigned to the reduction of Fe_2O_3 to Fe_3O_4 (Chen et al., 2014; Pan et al., 2016) and the peak at 524 °C can be attributed to the co-reduction of Fe_2O_3 and Fe_3O_4 to FeO and Fe (Zhang et al., 2018; Zou et al., 2018). Finally, the peak at 770 °C can be due to the reduction of iron-phosphate (Chen et al., 2014) or the co-reduction of nickel and iron associated with phosphate (Pan et al., 2016).

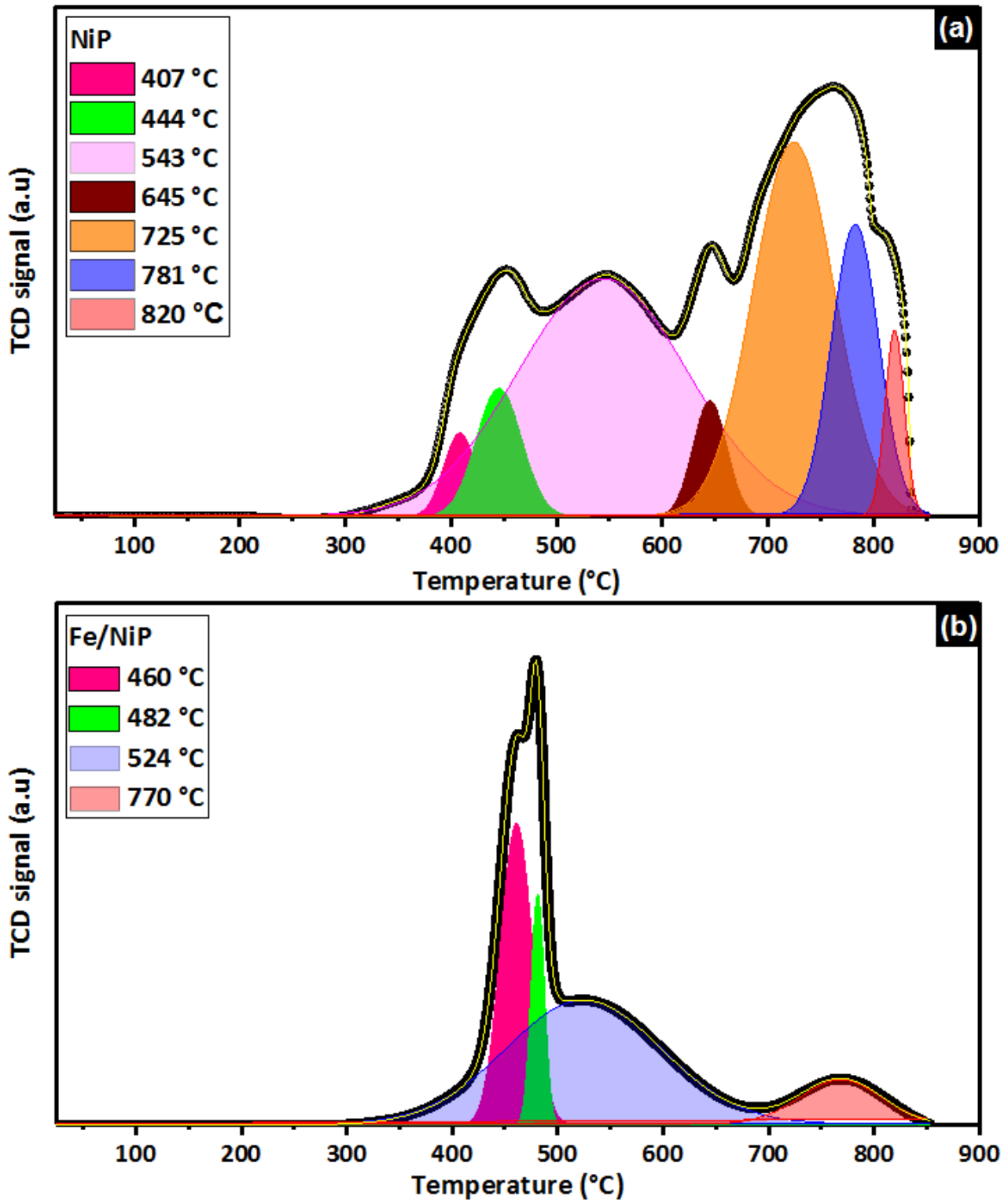


Fig. 2: H₂-Temperature Programmed Reduction profiles of (a) NiP (b) Fe/NiP.

The Transmission Electron Microscopy (TEM) images of NiP and Fe/NiP are shown in Fig.3.

As it can be seen in **Fig. 3a** and **3b**, NiP exhibits an amorphous nano-cylindrical morphology with different thicknesses ranging from 13 to 49 nm. In addition, the TEM images also indicate the presence of interconnected mesopores. The distribution of particle size is centered at 5.5 nm (**Fig. 3c**). In contrast, after the impregnation of Fe on NiP, the nano-cylindrical morphology and the porosity are not observed (**Fig. 3d**), this can be explained by the high dispersion of Fe (yellow color) on the surface of NiP. Indeed, the map analysis of the Fe/NiP sample (**Fig. 3e**) shows the homogenous distribution of Fe on the NiP surface. Furthermore, the mapping analysis reveals the presence of sulfur (green color), which is present in the active phase ($(\text{Fe}_{1.33}^{2+}\text{Fe}_{0.67}^{3+}(\text{SO}_4)_2(\text{OH})_{0.67} \cdot x\text{H}_2\text{O})$), already identified by XRD. This result is therefore in good agreement with N₂-physisorption analysis, which reveals a decrease in surface area due to the clogging of pores by Fe particles.

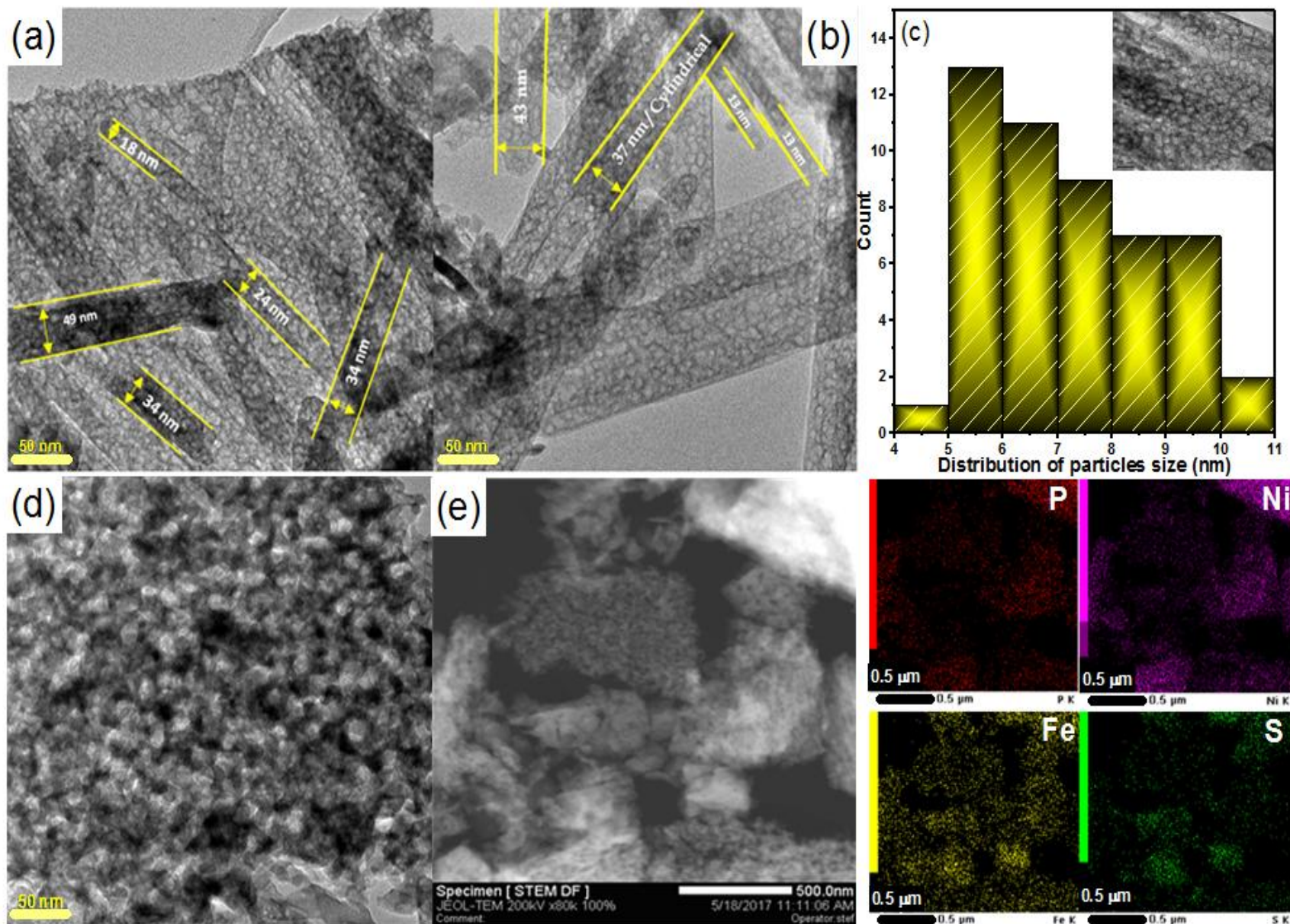


Fig. 3 (a) and (b): TEM images of NiP, (c): Distribution of particle size, (d): TEM of Fe/NiP, and (e): TEM-mapping.

3.2. Catalytic results

3.2.1. Thermal decomposition (blank tests)

The temperature plays a very important role in the WAO process of degradation of hazardous organic pollutants. Thus, the rate of reaction, the total reduction of TOC and COD are strongly dependent on the temperature (Kaplan et al., 2014b; Pintar et al., 2008). Moreover, the mechanism of degradation of organic pollutants in the WAO process is also strongly related to the reaction temperature due to the various types of free radicals that can be generated (Pintar et al., 2008). For this reason, blank experiments i.e without a catalyst, were carried out to study the thermal decomposition of BPA at 140°C. **Fig. 4a** displays BPA conversion as a function of time. Blank test shows that the conversion of BPA after 180 min at 140°C reaches only 37.0 % and leads to many by-products, as shown on the HPLC chromatogram displayed in **Fig. 4b**. This result is explained by the fact that the aromatic structure of the phenolic compounds gives them a high activation energy for WAO. Consequently, higher reaction temperature is required to get over such high activation energy barriers (Mirzaee et al., 2018). In order to avoid excessive temperature conditions and thus reduce the cost, the use of a catalyst is necessary to improve the conversion of BPA and to avoid the formation of by-products.

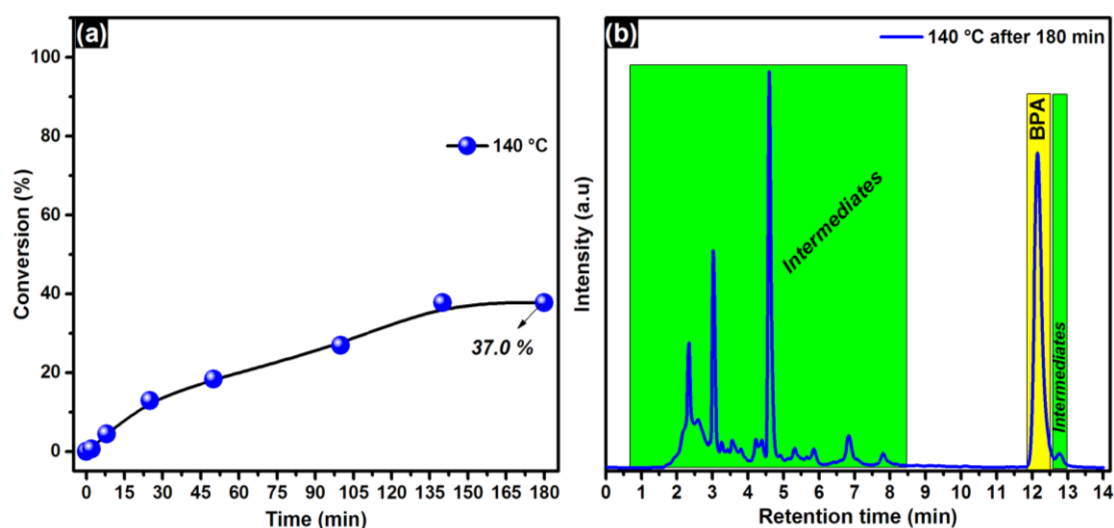


Fig. 4 (a) Thermal decomposition of BPA at 140 °C (b) HPLC chromatogram for WAO of BPA (without catalyst).

3.2.2. Effect of support and catalyst

First, the NiP support was tested to evaluate its performance for CWAQ of BPA. **Fig. 5a** shows that BPA conversion after 180 min of reaction (37 %) is similar to that obtained with the blank test at 140°C. On the other hand, the modification of NiP by Fe induces a significant increase in catalytic properties. Fe/NiP exhibits a good catalytic activity since the BPA is fully converted (99.8 %) after

180 min of reaction (**Fig. 5a**) and 85 % Δ TOC are achieved (**Table 2**) versus only 35 % with NiP. Nevertheless, BPA was not entirely transformed into carbon dioxide, which implies the formation of some organic intermediates.

Liquid phase samples were periodically collected during the CWAO process for analysis by HPLC for the blank test, NiP and Fe/NiP. The conversion curves are displayed in Fig. 5a. The HPLC chromatograms focused on the BPA peaks were illustrated in **Fig. 5b, c and d**. The inset figures (**Fig. 5b, c and d**) showed the temporal evolution of the spectral changes of BPA generated by HPLC of BPA conversion using NiP and Fe/NiP samples. With the reaction time, the peak intensity of BPA gradually decreases. BPA is fully converted after 180 min for Fe/NiP. The disappearance of BPA is accompanied by the formation of its by-products similarly to that is observed in Fig. 4b. The formation of these by-products is in accordance with the values of Δ TOC.

Comparison of the HPLC chromatograms (**Fig. 6a, b**) after 180 min of reaction shows that several intermediates are detected in the case of NiP while only two peaks are detected in the case of Fe/NiP. These peaks are detected at a shorter retention time than that of BPA, indicating that the intermediates produced are more polar than BPA. This is in agreement with the results stated in the preview study on the degradation of BPA (Tai et al., 2005). However, all detected peak areas of the BPA intermediates were much lower than those of the initial BPA. In other words, fluctuations of these BPA intermediates as a function of time reveal different possible step in the degradation pathways of BPA, and it is, therefore, difficult to identify them. Although the study does not aim to analyze in detail the by-products obtained during the CWAO of BPA, the main products detected were tentatively identified in comparison to the studies of Miho Sasaki et al (Sasaki et al., 2005b, 2005a), Vincent Cleveland et al (Cleveland et al., 2014) and Buddhika Rathnayake et al (Rathnayake et al., 2019). Thus, the HPLC analysis (**Fig. 6c**) of BPA solution treated by CWAO using Fe/NiP at 140°C after 180 min revealed the formation of two intermediates: 4'-hydroxyacetophenone and 1,2-bis(4-hydroxyphenyl)-2-propanol.

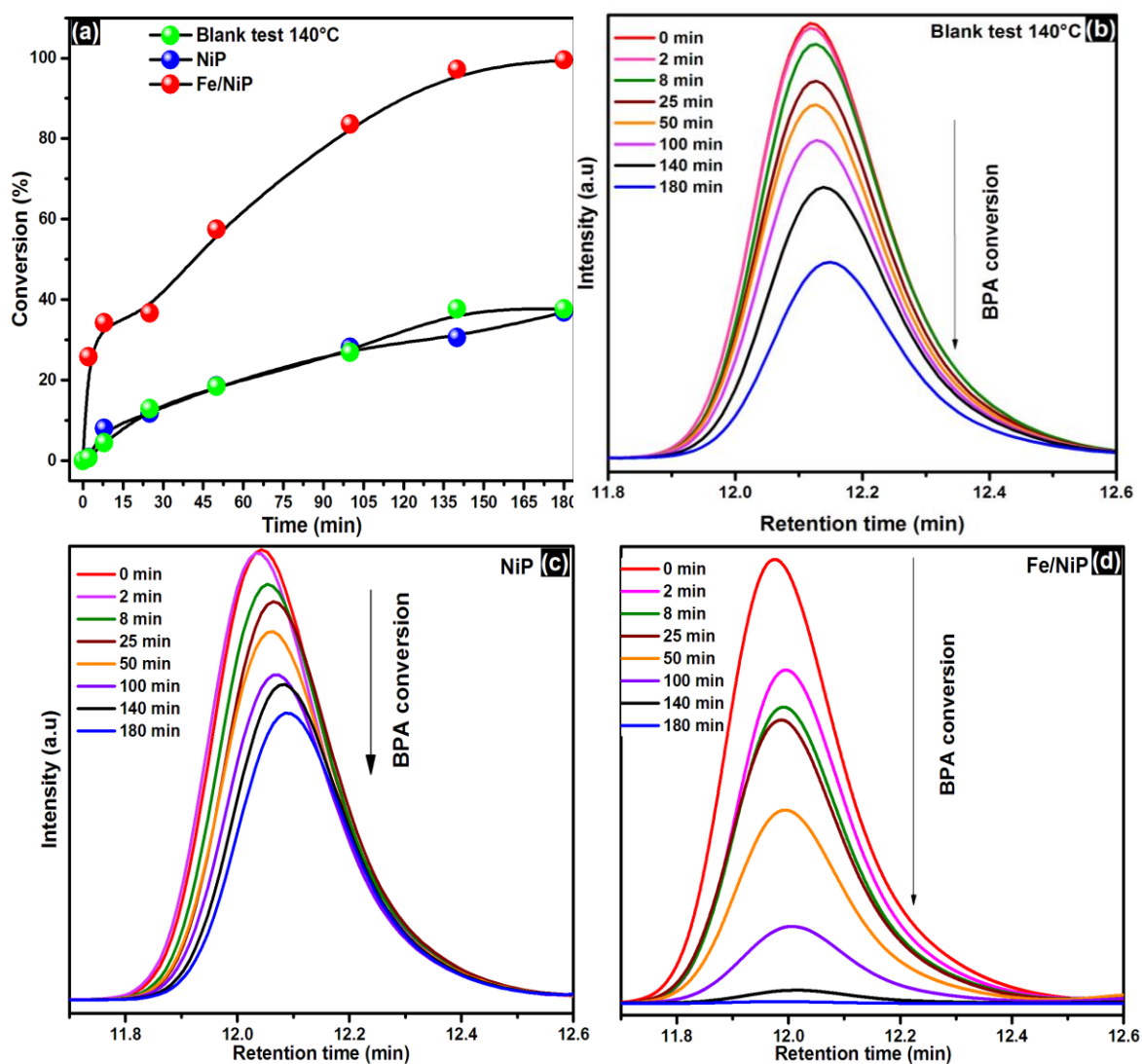
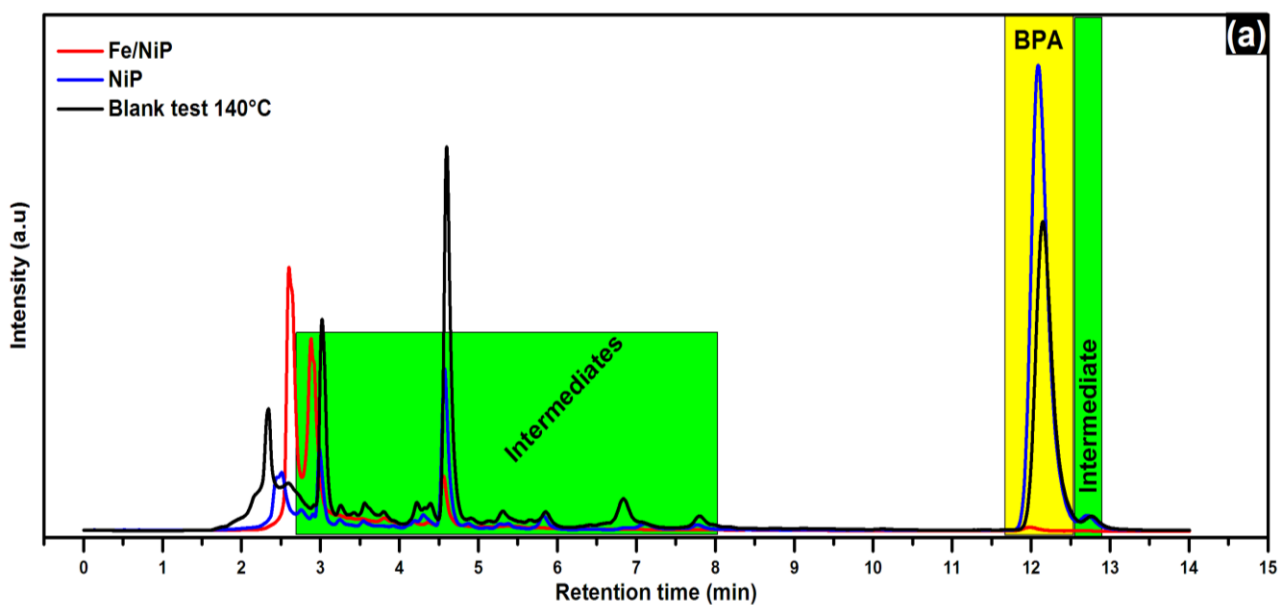


Fig. 5: (a) Kinetics of BPA conversion (%), (b) HPLC **chromatograms focused on BPA** without catalyst at 140°C (c) using NiP, (d) using Fe/NiP.



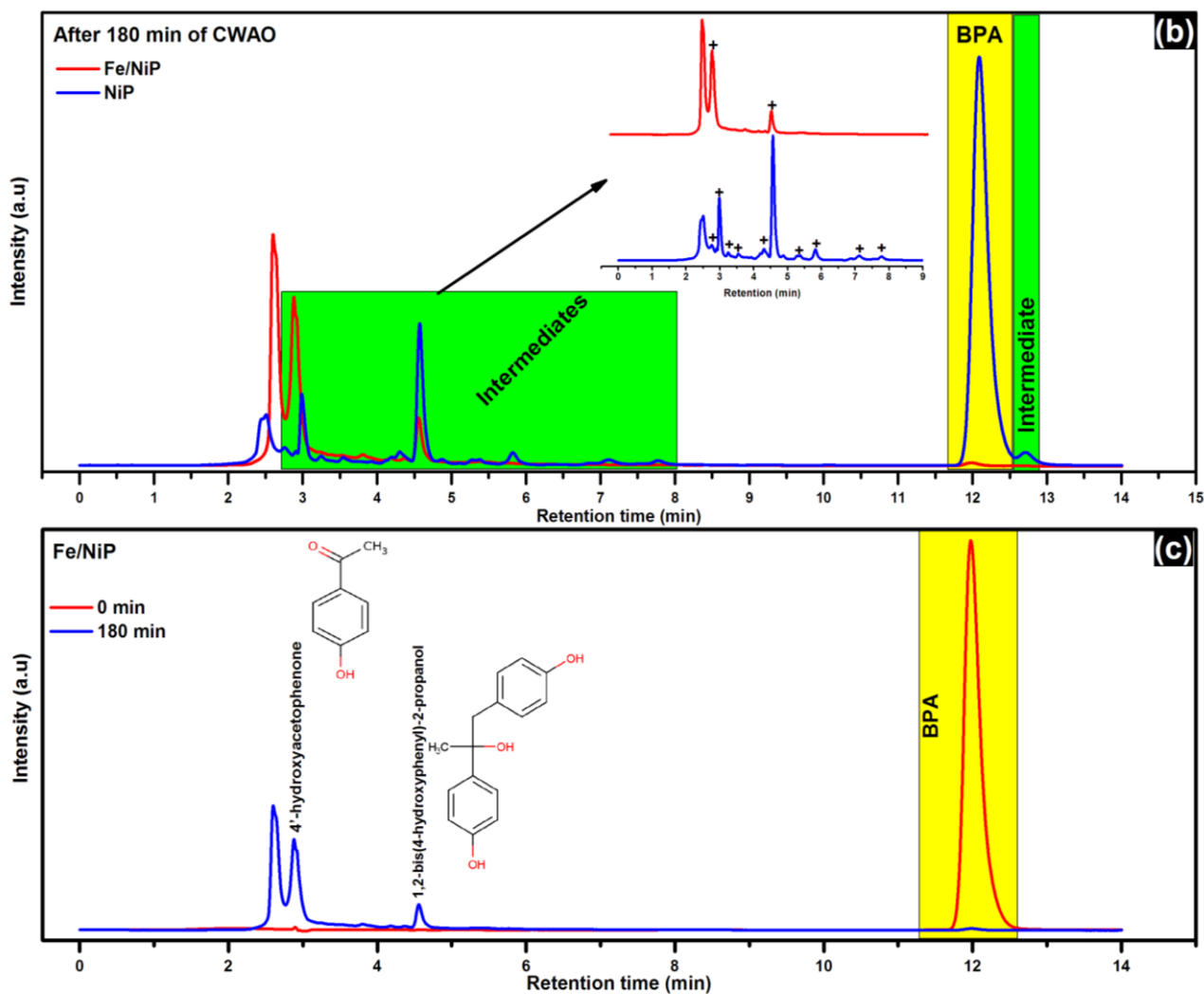


Fig.6: Intermediates detection by HPLC analysis during CWAO of BPA: (a) comparison between the blank test at 140°C, NiP and Fe/NiP after 180 min of reaction, (b) comparison between NiP and Fe/NiP after 180 min of reaction, (c) comparison after 0 and 180 min reaction time for Fe/NiP.

3.2.3. Kinetic modeling of CWAO reaction of BPA

The kinetics of BPA CWAO reaction was modeled according to the pseudo-first-order (PFO) rate-law. The measured data were fitted by using a non-linear model, according to the following equation (Equ.1):

$$C(t) = C_{tot}(1 - e^{-kt}) \quad \text{Equ.1}$$

Where the total conversion (C_{tot}) and the rate constant (k) were used as fitting parameters. The term “ t ” was the CWAO reaction time. The calculated R^2 values and the residual analysis were used as parameters to evaluate the quality of the fit. Fig. 7 displays both the experimental and fitted BPA conversion as a function of reaction time for NiP and Fe/NiP. The possible rate constants for NiP and Fe/NiP would be 0.014 and 0.020 min^{-1} , respectively. Therefore, the addition of iron to NiP clearly enhanced the conversion of BPA and the rate of reaction.

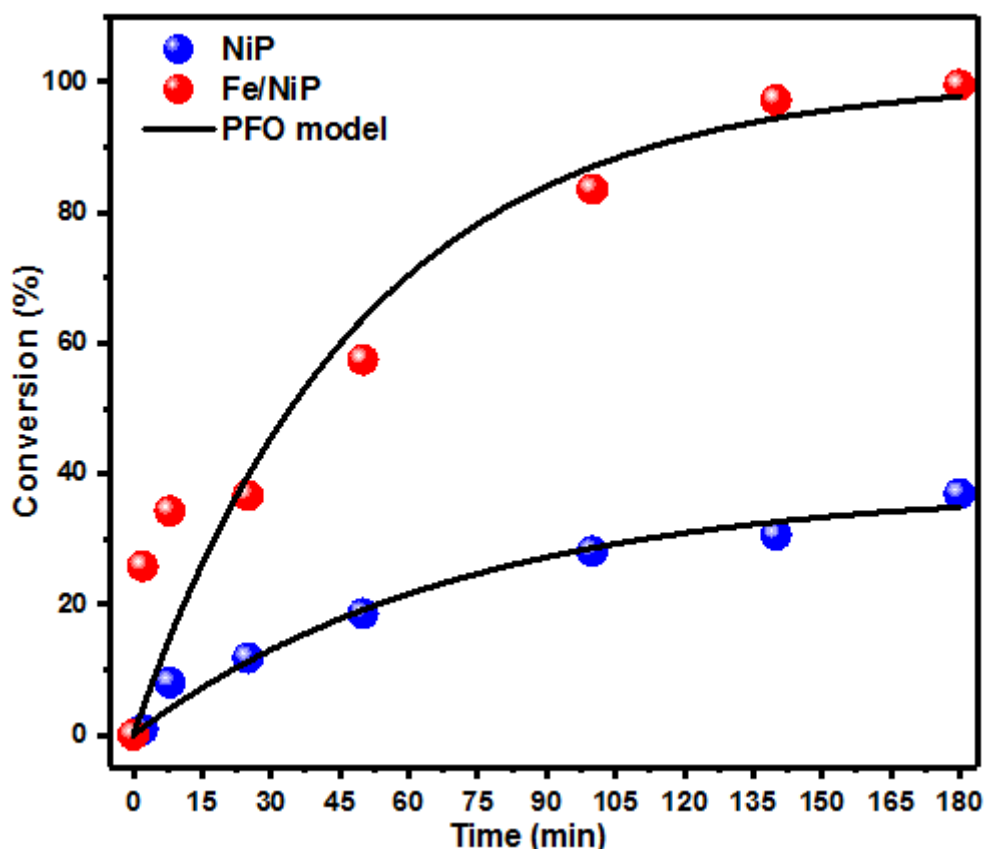


Fig. 7 Pseudo-first-order kinetic fitting of BPA conversion for NiP and Fe/NiP.

3.2.4. Stability test

In addition to being efficient for the CWAQ reaction, the catalyst must be stable under the operating conditions. To evaluate the stability of the Fe/NiP catalyst, it was reused three times in consecutive CWAQ reactions. Once the catalyst was removed from the autoclave, it was filtered, washed with ultrapure water and then dried in the oven at 60°C.

Fig. 8 shows that the BPA conversion remains at about 99% after 3 cycles. However, the efficiency of the solid declines over the multiple cycles since the % Δ TOC decreases which could be due to the accumulation of intermediates and by-products onto Fe/NiP surface. Furthermore, the ICP analysis of the remaining solution after each cycle shows negligible leaching of iron (**Table 2**), indicating high stability of iron in the prepared catalyst (Fe/NiP). Nickel leaching is also negligible: 860 ppm (0.08 wt-%) after the first cycle and around 60-75 ppm for each subsequent cycles.

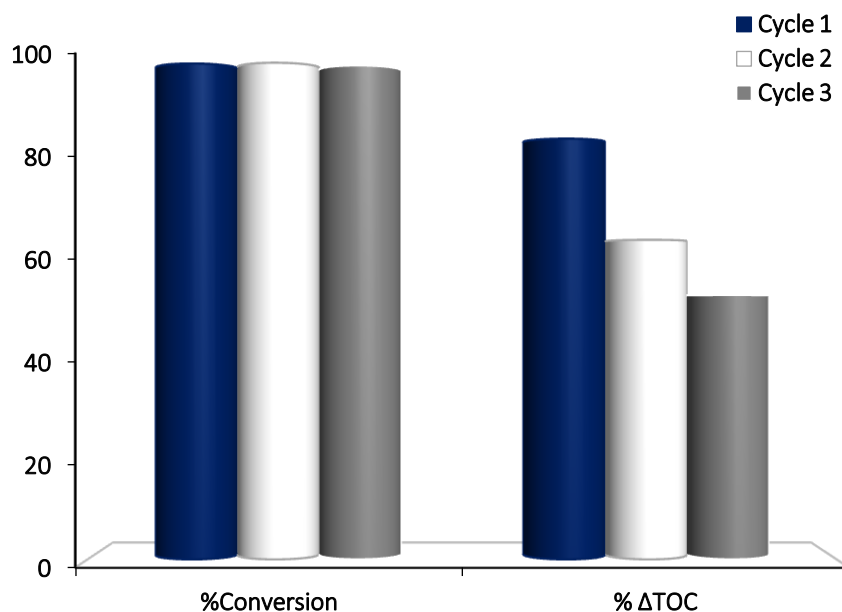


Fig. 8 Catalytic performance of Fe/NiP reused three times in consecutive CWAO reactions. Conversion of BPA and TOC abatement (Δ TOC) after 180 min of reaction.

Table 2. Metal leaching after 180 min of CWAO of BPA using the catalyst Fe/NiP.

leaching	Cycle 1	Cycle 2	Cycle 3
[Fe] (ppm)	0.03	0.03	0.02
[Ni] (ppm)	859.50	60.80	74.80

The diffractograms of the catalysts after each cycle (**Fig. 9**) reveal the disappearance of the $\text{Fe}_2(\text{SO}_4)_2(\text{OH})_{0.67} \cdot x\text{H}_2\text{O}$ (ICDD: 00-053-1056) phase and the appearance of a new $\text{Fe}_3(\text{PO}_4)_2(\text{OH})_2$ (ICDD: 00-014-0569) phase. The $\text{Ni}_3(\text{PO}_4)_2$ (ICDD: 00-038-1473) phase is also present in either crystalline or amorphous form, which seems to promote the conversion of BPA. In order to verify the synergistic effect between the iron phase and the nickel phase, an FeP catalyst was prepared using the same method of preparation as for the NiP catalyst. This catalyst was then evaluated for the CWAO of BPA. The results obtained are summarized in **Table 3**. Although the FeP catalyst has a high conversion of BPA, very close to that of Fe/NiP, the presence of the nickel phase in Fe/NiP results in a higher Δ TOC, around 85.0%. It can be concluded that the iron phase enables almost total conversion of BPA, but the addition of nickel is necessary to promote total oxidation.

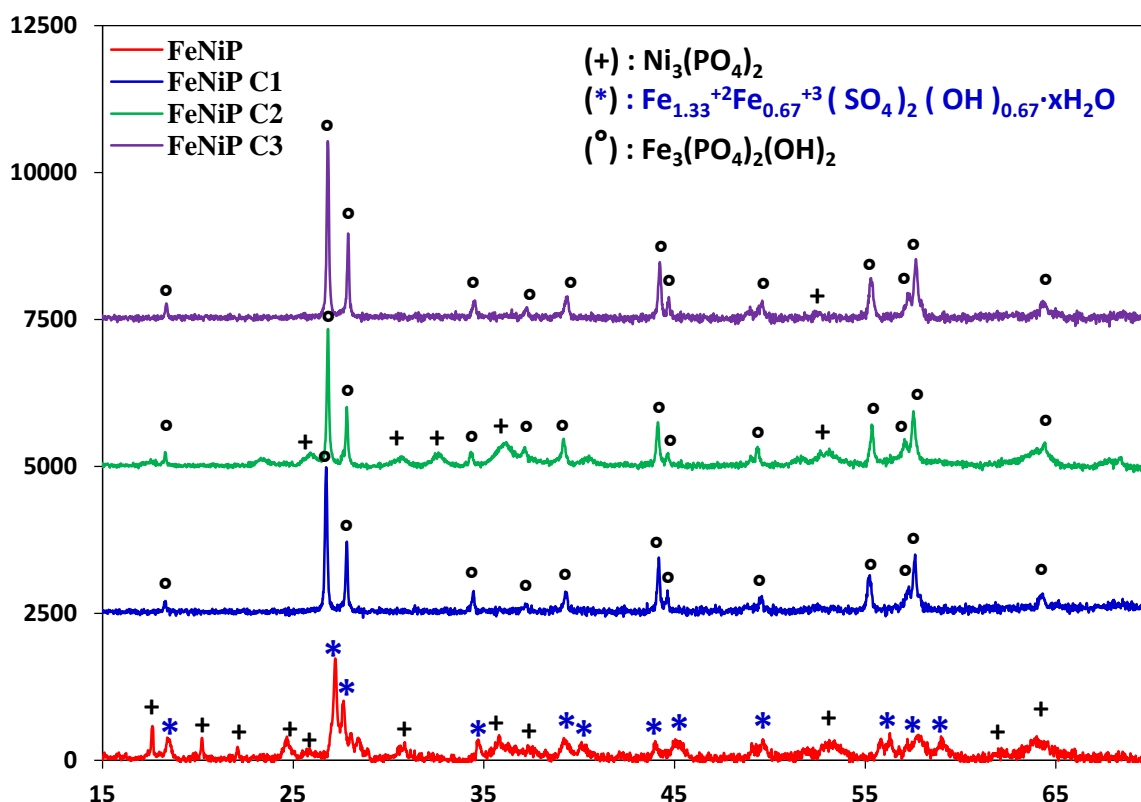


Fig. 9 XRD patterns of Fe/NiP after 180 min of CWAO of BPA for three cycles.

Table 3. Conversion of Bisphenol A and Δ TOC after 180 min at 140 °C.

Sample	BPA conversion (%)	% Δ TOC
NiP	37.0	35.0
Fe/NiP	99.6	85.0
FeP	99.7	64.4

3.2.5. Comparison of our results to other works

Table 4 provides a comparison of our results with those reported in the literature for the CWAO of BPA. It appears that the Fe/NiP material has better catalytic performance, both in terms of conversion and TOC abatement (Δ TOC).

Table 4. Comparison of CWAO of BPA conversion and Δ TOC on different catalysts.

Catalyst	BPA initial concentration (mg/L)	Temperature (°C)	Time (min)	Conversion (%)	% Δ TOC	References
CeO ₂	60	160	180	76	75	(Heponiemi et al., 2015)
Ce _{0.85} Zr _{0.15} O ₂	60	160	180	76	73	(Heponiemi et al., 2015)

Titanate nanotube	10	200	Severa l hours	91	69	(Kaplan et al., 2014b)
Ru/CNS	20	130	90	>99	nd	(Serra-Pérez et al., 2019);
Pt/0.8Ti-0.2Ce	60	160	180	72	48	(Rathnayake et al., 2019)
Fe/NiP	300	140	180	>99	85	This work

nd : not determined : For the Ru/CNS the Δ TOC it is not mentioned in the publication

4. Conclusion

The catalytic wet air oxidation of BPA was investigated by nickel phosphate as support (NiP) and iron supported on NiP as a catalyst. The conversion of BPA was studied at 140°C and 25 bar of total pressure. The CWAO reaction using Fe/NiP catalyst was effective in achieving almost complete conversion of BPA in 180 min of reaction. Moreover, Fe/NiP catalyst showed rather high stability given the severe operating conditions (acidic media, high pressure, high temperature) and was still highly effective in successive runs. We also demonstrated that FeP and Fe/NiP have high and similar activity, but the presence of the Ni phase ($\text{Ni}_3(\text{PO}_4)_2$) leads to a higher Δ TOC.

Studies are still ongoing in order to provide further insight into the CWAO of BPA for possible practical application.

Conflict of interest

The authors declare no conflict of interest

References

- Ahmadi, M., Rahmani, H., Takdastan, A., Jaafarzadeh, N., Mostoufi, A., 2016. A novel catalytic process for degradation of bisphenol A from aqueous solutions: A synergistic effect of nano- $\text{Fe}_3\text{O}_4@\text{Alg-Fe}$ on $\text{O}_3/\text{H}_2\text{O}_2$. *Process Saf. Environ. Prot.* 104, 413–421. <https://doi.org/10.1016/j.psep.2016.09.008>
- Akbari, S., Ghanbari, F., Moradi, M., 2016. Bisphenol A degradation in aqueous solutions by electrogenerated ferrous ion activated ozone, hydrogen peroxide and persulfate: Applying low current density for oxidation mechanism. *Chem. Eng. J.* 294, 298–307. <https://doi.org/10.1016/j.cej.2016.02.106>
- Anastopoulos, I., Anagnostopoulos, V.A., Bhatnagar, A., Mitropoulos, A.C., Kyzas, G.Z., 2017. A review for chromium removal by carbon nanotubes. *Chem. Ecol.* 33, 572–588. <https://doi.org/10.1080/02757540.2017.1328503>

- Arampatzidou, A., Voutsas, D., Deliyanni, E., 2018. Removal of bisphenol A by Fe-impregnated activated carbons. *Environ. Sci. Pollut. Res. Int.* 25, 25869–25879. <https://doi.org/10.1007/s11356-018-2652-4>
- Athalathil, S., Erjavec, B., Kaplan, R., Stüber, F., Bengoa, C., Font, J., Fortuny, A., Pintar, A., Fabregat, A., 2015. TiO₂-sludge carbon enhanced catalytic oxidative reaction in environmental wastewaters applications. *J. Hazard. Mater.* 300, 406–414. <https://doi.org/10.1016/j.jhazmat.2015.07.025>
- Ben-Jonathan, N., Steinmetz, R., 1998. Xenoestrogens: the emerging story of bisphenol a. *Trends Endocrinol. Metab.* TEM 9, 124–128. [https://doi.org/10.1016/s1043-2760\(98\)00029-0](https://doi.org/10.1016/s1043-2760(98)00029-0)
- Bui, P., Cecilia, J.A., Oyama, S.Ted., Takagaki, A., Infantes-Molina, A., Zhao, H., Li, D., Rodríguez-Castellón, E., Jiménez López, A., 2012. Studies of the synthesis of transition metal phosphides and their activity in the hydrodeoxygenation of a biofuel model compound. *J. Catal.* 294, 184–198. <https://doi.org/10.1016/j.jcat.2012.07.021>
- Chapin, R.E., Adams, J., Boekelheide, K., Gray, L.E., Hayward, S.W., Lees, P.S.J., McIntyre, B.S., Portier, K.M., Schnorr, T.M., Selevan, S.G., Vandenbergh, J.G., Woskie, S.R., 2008. NTP-CERHR expert panel report on the reproductive and developmental toxicity of bisphenol A. *Birth Defects Res. B. Dev. Reprod. Toxicol.* 83, 157–395. <https://doi.org/10.1002/bdrb.20147>
- Chen, J., Shi, H., Li, L., Li, K., 2014. Deoxygenation of methyl laurate as a model compound to hydrocarbons on transition metal phosphide catalysts. *Appl. Catal. B Environ.* 144, 870–884. <https://doi.org/10.1016/j.apcatb.2013.08.026>
- Chouhan, S., Prakash, J., Swati, Singh, S.P., 2014. Effect of Bisphenol A on human health and its degradation by microorganisms: a review. *Ann. Microbiol.* 64, 13–21. <https://doi.org/10.1007/s13213-013-0649-2>
- Cleveland, V., Bingham, J.-P., Kan, E., 2014. Heterogeneous Fenton degradation of bisphenol A by carbon nanotube-supported Fe₃O₄. *Sep. Purif. Technol.* 133, 388–395. <https://doi.org/10.1016/j.seppur.2014.06.061>
- Erjavec, B., Kaplan, R., Djinović, P., Pintar, A., 2013. Catalytic wet air oxidation of bisphenol A model solution in a trickle-bed reactor over titanate nanotube-based catalysts. *Appl. Catal. B Environ.* 132–133, 342–352. <https://doi.org/10.1016/j.apcatb.2012.12.007>
- Gültekin, I., Ince, N.H., 2007. Synthetic endocrine disruptors in the environment and water remediation by advanced oxidation processes. *J. Environ. Manage.* 85, 816–832. <https://doi.org/10.1016/j.jenvman.2007.07.020>

- Heponiemi, A., Azalim, S., Hu, T., Lassi, U., 2015. Cerium Oxide Based Catalysts for Wet Air Oxidation of Bisphenol A. *Top. Catal.* 58, 1043–1052. <https://doi.org/10.1007/s11244-015-0457-y>
- Kaplan, R., Erjavec, B., Senila, M., Pintar, A., 2014a. Catalytic wet air oxidation of bisphenol A solution in a batch-recycle trickle-bed reactor over titanate nanotube-based catalysts. *Environ. Sci. Pollut. Res.* 21, 11313–11319. <https://doi.org/10.1007/s11356-014-3042-1>
- Kaplan, R., Erjavec, B., Senila, M., Pintar, A., 2014b. Catalytic wet air oxidation of bisphenol A solution in a batch-recycle trickle-bed reactor over titanate nanotube-based catalysts. *Environ. Sci. Pollut. Res. Int.* 21, 11313–11319. <https://doi.org/10.1007/s11356-014-3042-1>
- Keav, S., de los Monteros, A.E., Barbier, J., Duprez, D., 2014. Wet Air Oxidation of phenol over Pt and Ru catalysts supported on cerium-based oxides: Resistance to fouling and kinetic modelling. *Appl. Catal. B Environ.* 150–151, 402–410. <https://doi.org/10.1016/j.apcatb.2013.12.028>
- Kim, K.-H., Ihm, S.-K., 2011. Heterogeneous catalytic wet air oxidation of refractory organic pollutants in industrial wastewaters: A review. *J. Hazard. Mater.* 186, 16–34. <https://doi.org/10.1016/j.jhazmat.2010.11.011>
- Lane, R.F., Adams, C.D., Randtke, S.J., Carter, R.E., 2015. Chlorination and chloramination of bisphenol A, bisphenol F, and bisphenol A diglycidyl ether in drinking water. *Water Res.* 79, 68–78. <https://doi.org/10.1016/j.watres.2015.04.014>
- Lee, S., Liao, C., Song, G.-J., Ra, K., Kannan, K., Moon, H.-B., 2015. Emission of bisphenol analogues including bisphenol A and bisphenol F from wastewater treatment plants in Korea. *Chemosphere* 119, 1000–1006. <https://doi.org/10.1016/j.chemosphere.2014.09.011>
- Levec, J., Pintar, A., 2007. Catalytic wet-air oxidation processes: A review. *Catal. Today* 124, 172–184. <https://doi.org/10.1016/j.cattod.2007.03.035>
- Lobos, J.H., Leib, T.K., Su, T.M., 1992. Biodegradation of bisphenol A and other bisphenols by a gram-negative aerobic bacterium. *Appl. Environ. Microbiol.* 58, 1823–1831.
- Mirzaee, S.A., Jaafarzadeh, N., Jorfi, S., Gomes, H.T., Ahmadi, M., 2018. Enhanced degradation of Bisphenol A from high saline polycarbonate plant wastewater using wet air oxidation. *Process Saf. Environ. Prot.* 120, 321–330. <https://doi.org/10.1016/j.psep.2018.09.021>
- Mohapatra, D.P., Brar, S.K., Tyagi, R.D., Surampalli, R.Y., 2010. Physico-chemical pre-treatment and biotransformation of wastewater and wastewater Sludge – Fate of bisphenol A. *Chemosphere* 78, 923–941. <https://doi.org/10.1016/j.chemosphere.2009.12.053>
- Moussavi, G., Pourakbar, M., Shekoohiyan, S., Satari, M., 2018. The photochemical decomposition and detoxification of bisphenol A in the VUV/H₂O₂ process: Degradation, mineralization,

and cytotoxicity assessment. Chem. Eng. J. 331, 755–764.
<https://doi.org/10.1016/j.cej.2017.09.009>

Nousir, S., Keav, S., Barbier, J., Bensitel, M., Brahmi, R., Duprez, D., 2008. Deactivation phenomena during catalytic wet air oxidation (CWAO) of phenol over platinum catalysts supported on ceria and ceria–zirconia mixed oxides. Appl. Catal. B Environ. 84, 723–731.
<https://doi.org/10.1016/j.apcatb.2008.06.010>

Omoike, A., Wacker, T., Navidonski, M., 2013. Biodegradation of bisphenol A by *Heliscus lugdunensis*, a naturally occurring hyphomycete in freshwater environments. Chemosphere 91, 1643–1647. <https://doi.org/10.1016/j.chemosphere.2012.12.045>

Pan, Z., Wang, R., Nie, Z., Chen, J., 2016. Effect of a second metal (Co, Fe, Mo and W) on performance of Ni₂P/SiO₂ for hydrodeoxygenation of methyl laurate. J. Energy Chem. 25, 418–426. <https://doi.org/10.1016/j.jechem.2016.02.007>

Pintar, A., Batista, J., Tišler, T., 2008. Catalytic wet-air oxidation of aqueous solutions of formic acid, acetic acid and phenol in a continuous-flow trickle-bed reactor over Ru/TiO₂ catalysts. Appl. Catal. B Environ. 84, 30–41. <https://doi.org/10.1016/j.apcatb.2008.03.001>

Rathnayake, B., Heponiemi, A., Huovinen, M., Ojala, S., Pirilä, M., Loikkanen, J., Azalim, S., Saouabe, M., Brahmi, R., Vähäkangas, K., Lassi, U., Keiski, R.L., 2019. Photocatalysis and catalytic wet air oxidation: Degradation and toxicity of bisphenol A containing wastewaters. Environ. Technol. 1–12. <https://doi.org/10.1080/09593330.2019.1604817>

Reddy, P.V.L., Kim, K.-H., 2015. A review of photochemical approaches for the treatment of a wide range of pesticides. J. Hazard. Mater. 285, 325–335.
<https://doi.org/10.1016/j.jhazmat.2014.11.036>

Sasaki, M., Akahira, A., Oshiman, K., Tsuchido, T., Matsumura, Y., 2005a. Purification of Cytochrome P450 and Ferredoxin, Involved in Bisphenol A Degradation, from *Sphingomonas* sp. Strain AO1. Appl. Environ. Microbiol. 71, 8024–8030.
<https://doi.org/10.1128/AEM.71.12.8024-8030.2005>

Sasaki, M., Maki, J., Oshiman, K., Matsumura, Y., Tsuchido, T., 2005b. Biodegradation of bisphenol A by cells and cell lysate from *Sphingomonas* sp. strain AO1. Biodegradation 16, 449–459. <https://doi.org/10.1007/s10532-004-5023-4>

Serra-Pérez, E., Álvarez-Torrellas, S., Ismael Águeda, V., Delgado, J.A., Ovejero, G., García, J., 2019. Insights into the removal of Bisphenol A by catalytic wet air oxidation upon carbon nanospheres-based catalysts: Key operating parameters, degradation intermediates and reaction pathway. Appl. Surf. Sci. 473, 726–737.
<https://doi.org/10.1016/j.apsusc.2018.12.205>

- Sing, K.S.W., 1985. Reporting physisorption data for gas/solid systems with special reference to the determination of surface area and porosity (Recommendations 1984). *Pure Appl. Chem.* 57, 603–619. <https://doi.org/10.1351/pac198557040603>
- Staples, C.A., Dome, P.B., Klecka, G.M., Oblock, S.T., Harris, L.R., 1998. A review of the environmental fate, effects, and exposures of bisphenol A. *Chemosphere* 36, 2149–2173. [https://doi.org/10.1016/S0045-6535\(97\)10133-3](https://doi.org/10.1016/S0045-6535(97)10133-3)
- Tai, C., Jiang, G., Liu, Jingfu, Zhou, Q., Liu, Jiyan, 2005. Rapid degradation of bisphenol A using air as the oxidant catalyzed by polynuclear phthalocyanine complexes under visible light irradiation. *J. Photochem. Photobiol. Chem.* 172, 275–282. <https://doi.org/10.1016/j.jphotochem.2004.12.015>
- Thommes, M., 2010. Physical Adsorption Characterization of Nanoporous Materials. *Chem. Ing. Tech.* 82, 1059–1073. <https://doi.org/10.1002/cite.201000064>
- Vandenberg, L.N., Hauser, R., Marcus, M., Olea, N., Welshons, W.V., 2007. Human exposure to bisphenol A (BPA). *Reprod. Toxicol.* 24, 139–177. <https://doi.org/10.1016/j.reprotox.2007.07.010>
- Zbair, M., Ainassaari, K., El Assal, Z., Ojala, S., El Ouahedy, N., Keiski, R.L., Bensitel, M., Brahmi, R., 2018. Steam activation of waste biomass: highly microporous carbon, optimization of bisphenol A, and diuron adsorption by response surface methodology. *Environ. Sci. Pollut. Res.* 25, 35657–35671. <https://doi.org/10.1007/s11356-018-3455-3>
- Zhang, Z., Huang, J., Xia, H., Dai, Q., Gu, Y., Lao, Y., Wang, X., 2018. Chlorinated volatile organic compound oxidation over SO₄²⁻/Fe₂O₃ catalysts. *J. Catal.* 360, 277–289. <https://doi.org/10.1016/j.jcat.2017.11.024>
- Zou, X., Chen, T., Zhang, P., Chen, D., He, J., Dang, Y., Ma, Z., Chen, Y., Toloueinia, P., Zhu, C., Xie, J., Liu, H., Suib, S.L., 2018. High catalytic performance of Fe-Ni/Palygorskite in the steam reforming of toluene for hydrogen production. *Appl. Energy* 226, 827–837. <https://doi.org/10.1016/j.apenergy.2018.06.005>